Numerical Studies on Supersonic Fluid Flow past a Cavity Involving Pressure Field and Aeroacoustic Effects Using LES Approach

Dr. Nirmal Kumar Kund
Associate Professor, Department of Production Engineering, Veer Surendra Sai University of Technology, Burla 768018, India

Abstract – An appropriate numerical model is presented to compute supersonic flow over a three-dimensional open cavity. The investigations of supersonic flow over the three-dimensional cavity having length-to-depth ratio of 2, encompass the supersonic free-stream Mach number of 2 and the flow Reynolds number of 10^5. The numerical simulation has been performed by using the Large Eddy Simulation (LES) approach. The Smagorinky model is employed for this study. The results obtained have been compared with the experimental data and numerical simulation predictions existing in the literature. The results have been presented in the form of both coefficient of pressure (Cp) and overall sound pressure level (OASPL). The coefficient of pressure seems to match qualitatively with the available experimental and numerical results reported by the other researchers. However, the overall sound pressure level is over-predicted by nearly 30-50 dB. In addition, the feedback loop mechanism of the cavity has also been studied. Quite large pressure fluctuations are observed inside the cavity and hence these need to be reduced. However, the incorporation of a spoiler is also planned for future to change the flow features (inside the cavity) that can lead to the suppression/reduction in both pressure oscillations and overall sound pressure level inside the cavity.

Index Terms – Numerical, Supersonic, Cavity, LES, Coefficient of Pressure, OASPL

1. INTRODUCTION

The existence of irregular structures or unsteady flow causes considerable aerodynamic noise leading to aero-acoustic resonance. It is due to the aerodynamic forces acting on the surface caused by air flow. This is witnessed in our everyday life such as exhaust pipes, vacuum cleaners, ventilation systems, fans etc. Noise generated by a flow is a major problem in many engineering applications (pertaining to surface transport, aviation and marine applications) like military vehicles, submarines, aircrafts, automobiles, etc. It can cause discomfort to humans and also affect the stealth of operations/performances.

Airframe noise (which is generated due to large pressure fluctuations inside the gear box) is a considerable component of overall noise, particularly during landing and take-off. Noise from landing gear, flaps, slats etc. are regarded as airframe noise. One of the most significant airframe noises is the cavity noise. They arise from open wheel wells after the undercarriage during landing. The weapon bays in the military aircrafts experience oscillations induced by the flow, which can excite the vibrational modes of the structure of the aircraft. At low Mach numbers for ground transportation, the automobile company is bothered with the noises generated from the door gaps, side mirrors, and the open sun roof. These noises generations also affect the comfort in the car.

The door gaps, wheel wells and weapon bays can be modelled as rectangular cavities and the composed flow outside the cavity can be regarded to be uniform. Though the rectangular cavity is elementary in shape, it is rich in diverse dynamic and acoustic phenomena, obscured by a possible aeroacoustic feedback loop depending on the shape/size of the cavity as well as the flow conditions. Severe tone noises may be produced because of the vortex shredding at the upstream edge of the cavity, during the flow past a cavity.

2. LITERATURE REVIEW

Heller et al. [1] investigated on flow-induced pressure oscillations in shallow cavities. Tam and Block [2] studied on the tones and pressure oscillations induced by flow over rectangular cavities. Kaufman et al. [3] reported on Mach 0.6 to 3.0 flows over rectangular cavities. Sweby [4] applied high resolution schemes using flux limiters on hyperbolic conservation laws. Rizzetta [5] performed numerical simulation on supersonic flow over a three-dimensional cavity. Anderson and Wendt [6] described about the fundamentals of computational fluid dynamics. Piomelli [7] demonstrated on achievements and challenges of large-eddy simulation. Hamed et al. [8] conducted numerical simulations of fluidic control for transonic cavity flows. Li et al. [9] carried out LES study of feedback-loop mechanism of supersonic open cavity flows. Vijayakrishnan [10] executed a validation study on unsteady RANS computations of supersonic flow over two dimensional cavity. Sousa et al. [11] discussed about the lid-driven cavity flow of viscoelastic liquids**.** Tuerke et al. [12] illustrated experimental study on double-cavity flow. It is realized that an extensive study on

cavity flow has been done both experimentally and computationally for improving the aerodynamic performance. However, besides its importance, the complicated flow physics of flow past a cavity has fascinated the investigators for further studies and remains to be an intense area of research.

Even though, the flow past a cavity has been studied experimentally/numerically by many researchers, but, complete modelling of both large and small scales of motions altogether, not yet done which is one of the major shortcomings. However, Large Eddy Simulation (LES) is the method which resolves the large eddies as it is and models the small eddies that can give reasonably more realistic results as well. The purpose of this research work is to study the flow physics and modes of oscillations in a three-dimensional open cavity supersonic flow. It involves details about the governing equations and the development along with the implementation of the LES technique including the sub-grid scale modelling. The discretization procedures have also been described. The simulation results have been presented in the form of pressure flow field, coefficient of pressure (Cp) and overall sound pressure level (OASPL). The simulation predictions of supersonic flow over an open cavity have also been compared with the existing experimental and numerical results available in the literature. In general, quite good agreement between the above stated results is also observed from the present investigations. However, the studies pertaining to the use of passive control techniques/devices for the suppression of pressure oscillations inside the cavity is planned for future. As these devices which operate over a wide range of parameters, significantly affect the flow physics of incoming boundary layer for extending equally effective flow situations.

3. DESCRIPTION OF PHYSICAL PROBLEM

Supersonic flow past a three-dimensional cavity is studied numerically. The streamwise length, depth and spanwise length of the cavity are 20 mm, 10 mm, and 10 mm, respectively. The length-to-depth ratio (L/D) for the cavity is 2. The width-to-depth ratio (W/D) is 1. The cavity is three-dimensional with streamwise length-to-spanwise length ratio (L/W) > 1. In addition, the Mach number of the free-stream along with the Reynolds number based on the cavity depth are taken as 2 and 10^5, respectively, for setting the inflow conditions.

3.1. Geometric Model

The computational domain of the cavity used in the present simulation is shown in figure 1. The size of the computational domain, as mentioned earlier, is 2D×D×D (length × breadth × width). The inlet boundary is located at a distance of D upstream from the leading edge of the cavity. The outlet boundary is located at a distance of 4D downstream from the trailing edge of the cavity. The upper boundary is also located at a distance of 4D above the cavity.

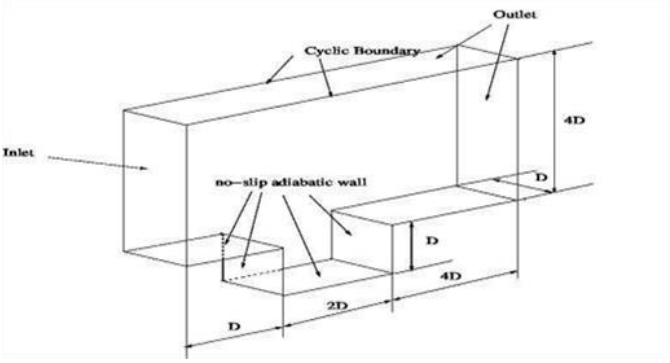

Fig 1. Computational domain of cavity

3.2. Initial and Boundary Conditions

The inflow boundary conditions are initialized with free-stream conditions of $M_\infty = 2$, $P_\infty = 101.325$ kPa, and $T_\infty = 300$ K. The Reynolds number of the flow used in the simulation is 10^5, which is based on the cavity depth. No-slip adiabatic wall boundary conditions is applied at the wall boundaries. Zero-gradient condition is applied at all the outflow boundaries. Periodical boundary condition is applied in the spanwise direction of the cavity.

4. MATHEMATICAL FORMULATION

4.1. Generalized governing transport equations

The three-dimensional compressible Navier-Stokes equations are the governing equations which include the continuity equation (1), the momentum equation (2), and the energy equation (3) which are as follows:

$$\frac{\partial \rho}{\partial t} + \nabla.(\rho \boldsymbol{U}) = 0 \quad (1)$$

$$\frac{\partial (\rho \boldsymbol{U})}{\partial t} + \nabla.(\rho \boldsymbol{U}.\boldsymbol{U}) - \nabla.\nabla(\mu \boldsymbol{U}) = -\nabla p \quad (2)$$

$$\frac{\partial (\rho e)}{\partial t} + \nabla.(\rho e \boldsymbol{U}) - \nabla.\nabla(\mu e) = -p(\nabla.\boldsymbol{U}) + \mu \left[\frac{1}{2}(\nabla \boldsymbol{U} + \nabla \boldsymbol{U}^{\mathrm{T}})\right]^2 \quad (3)$$

Where,

$\boldsymbol{U}$ = velocity vector = $u\hat{\imath} + v\hat{\jmath} + w\hat{k}$

$\frac{1}{2}(\nabla \boldsymbol{U} + \nabla \boldsymbol{U}^{\mathrm{T}})$ = strain rate tensor.

The equations (1), (2) and (3) represent the conservation form of the Navier-Stokes equations. The conservation form of these governing equations are achieved from a flow model fixed in space [6]. The above equations are applicable to viscous flow, except that the mass diffusion is no included.

It is assumed, in aerodynamics, that the gas is a perfect gas. The equation of state for a perfect gas is, $p = \rho RT$ (4)

Where, R = specific gas constant = C_p - C_v (5)

For a calorically perfect gas (constant specific heats), the caloric equation of state is,

e = internal energy per unit mass = C_vT (6)

4.2. LES Turbulence Modelling

The turbulent flows may be simulated using three different approaches: Reynolds-Averaged Navier-Stokes equations (RANS), direct numerical simulation (DNS), and large eddy simulation (LES). Direct numerical simulation has high computational requirements. DNS resolves all the scales of motion and for this it needs a number of grid points proportional to $(Re)^{9/4}$ and computational scales' cost is proportional to $(Re)^3$ [7].

In the present study, features of the turbulent flow field have been simulated using LES as it is appropriate for unsteady complex flows as well as noise induced flows. LES computes the large resolved scales and also models the smallest scales. The turbulence model is introduced by splitting the time and space varying flow variables into two constituents, the resolved one $\bar{f}$ and f', the unresolved part:

$$(x,t) = \bar{f}(x,t) + f'(x,t) \quad (7)$$

LES uses a filtering operation to separate these resolved scales from the unresolved scales. The filtered variable is denoted by an over bar [7]. The top-hat filter smooth both the fluctuations of the large-scale and those of small scales as well. The filtering operation when applied to the Navier-Stokes equation gives:

$$\frac{\partial \bar{\rho}}{\partial t} + \nabla.(\overline{\rho \boldsymbol{U}}) = 0 \quad (8)$$

$$\frac{\partial(\overline{\rho \boldsymbol{U}})}{\partial t} + \nabla.(\overline{\rho \boldsymbol{U}.\boldsymbol{U}}) - \nabla.\nabla(\overline{\mu \boldsymbol{U}}) = -\nabla \bar{p} \quad (9)$$

$$\frac{\partial(\overline{\rho e})}{\partial t} + \nabla.(\overline{\rho \boldsymbol{U} e}) - \nabla.\nabla(\overline{\mu e}) = -\overline{p(\nabla.\boldsymbol{U})} + \mu\left[\frac{1}{2}(\nabla \bar{\boldsymbol{U}} + \nabla \bar{\boldsymbol{U}}^{\mathrm{T}})\right]^2 \quad (10)$$

However, the dissipative scales of motion are rectified poorly by LES. In a turbulent flow, the energy from the large resolved structures are passed on to the smaller unresolved structures by an inertial and an effective inviscid mechanism. This is known as energy cascade. Hence, LES employs a sub-grid scale model to mimic the drain related to this energy cascade. Most of these models are eddy viscosity models relating the subgrid-scale stresses (τ_{ij}) and the resolved-scale rate of strain-tensor ($\bar{S}_{ij}$),

$$\tau_{ij} - (\delta_{ij}/3) = -2\nu_T \bar{S}_{ij} \quad (11)$$

Where, $\bar{S}_{ij}$ is the resolved-scale rate of strain tensor = $(\partial \bar{u}_i/\partial x_j + \partial \bar{u}_j/\partial x_i)/2$.

In most of the cases it is assumed that all the energy received by the unresolved-scales are dissipated instantaneously. This is the equilibrium assumption, i.e., the small-scales are in equilibrium [7]. This simplifies the problem to a great extent and an algebraic model is obtained for the eddy viscosity:

$$\mu_{sgs} = \rho C \Delta^2 |\bar{S}| \bar{S}_{ij},\ |\bar{S}| = (2\bar{S}_{ij}\bar{S}_{ij})^{1/2} \quad (12)$$

Here, Δ is the grid size and is usually taken to be the cube root of the cell volume [7]. This model is called as the Smagorinsky model and C is the Smagorinsky coefficient. In the present study, its value has been taken to be 0.2.

5. NUMERICAL PROCEDURES

5.1. Numerical scheme and solution algorithm

The three-dimensional compressible Navier-Stokes governing transport equations are discretized through a framework pertaining to finite volume method (FVM) using the SIMPLER algorithm. Here, the turbulent model used for large eddy simulation is Smagorinsky model, because of its simplicity. The spatial derivatives such as Laplacian and convective terms are computed by second order scheme based on Gauss theorem. In addition, the viscous terms are evaluated by second order scheme. Furthermore, the implicit second order scheme is used for time integration. The numerical fluxes are evaluated by applying Sweby limiter to central differencing (CD) scheme, which is a total variation diminishing (TVD) scheme. The central differencing (CD) is an unbounded second order scheme, whereas, the total variation diminishing (TVD) is a limited linear scheme. The established solver is used to predict flow behaviours of the associated flow variables relating to supersonic flow over an open cavity.

5.2. Choice of grid size, time step and convergence criteria

Figure 2 demonstrates that the computational domain comprises of two regions: upper cavity region and inside cavity region. The grid is refined at the regions near to the wall (where very high gradient is expected) to determine the behaviour of shear layer satisfactorily. A comprehensive grid-independence test is performed to establish a suitable spatial discretization, and the levels of iteration convergence criteria to be used. As an outcome of this test, the optimum number of grid points used for the final simulation, in the upper cavity region as 360 × 150 × 1 and those of in the inside cavity region as 200 × 150 × 1. Thus, the total number of grid points is 84000. The values of ΔX^+, ΔY^+ and ΔZ^+ at the leading edge of the cavity are 5, 12.5 and 1.0, respectively. Corresponding time step taken in the simulation is 0.000001 seconds. Though, it is checked with smaller grids of 132000 in

numbers, it is observed that a finer grid system does not alter the results significantly.

Convergence in inner iterations is declared only when the condition $\left|\frac{\varphi-\varphi_{old}}{\varphi_{max}}\right| \leq 10^{-4}$ is satisfied simultaneously for all variables, where φ stands for the field variable at a grid point at the current iteration level, φ_{old} represents the corresponding value at the previous iteration level, and φ_{max} is the maximum value of the variable at the current iteration level in the entire domain.

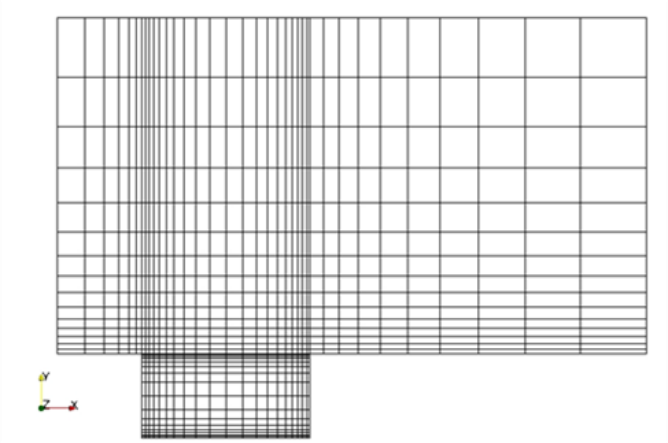

Fig 2. Computational grid of cavity in X-Y Plane

6. RESULTS AND DISCUSSIONS

6.1. Pressure distributions

The pressure fields at two different instants of times such as t = 0.2 sec and t = 0.4 sec are demonstrated in the figures 3 and 4, respectively. It is observed that a compression wave travelling forward reaches the front wall and part of the wave is reflected from the wall. This generates a reflection wave that travels backward. At the same time, another feedback compression wave propagates towards the front wall. At the centre part of the cavity, two large vortices are seen and these vortices convect towards the trailing edge of the cavity. Large structural vortices impinge on the aft wall and at the trailing edge there exists a high amplitude of pressure gradient.

The feedback compression wave, which reached at the front wall, then reaches at the lip of the leading edge and thereby, produces disturbance in the shear layer. The other feedback compression wave from the aft wall continues to propagate towards the front wall. The front vortex, out of the two vortices produced, induces inside the cavity and travels toward the aft wall. A new compression wave is produced at the aft wall edge and propagates upstream.

The generated reflection wave of feedback compression wave at the front wall and the feedback compression from the aft wall meet with each other inside the cavity. These continue to propagate towards their own direction. The front vortex, as mentioned earlier, impinges on the aft wall, and two shedding vortices behave energetically in the shear layer. Therefore, two shocks are formed, one at the leading edge and the other at the trailing edge.

The shedding vortex formed impinges on the trailing edge lip and is split into two parts, one of them convects downstream and the other part moves inside the cavity causing large mass injections. This recirculation flow affects the propagating direction of the front wall reflection compression wave travelling towards the aft wall. This compression wave becomes weak as it travels toward the aft wall and does not achieve high amplitude at the aft wall.

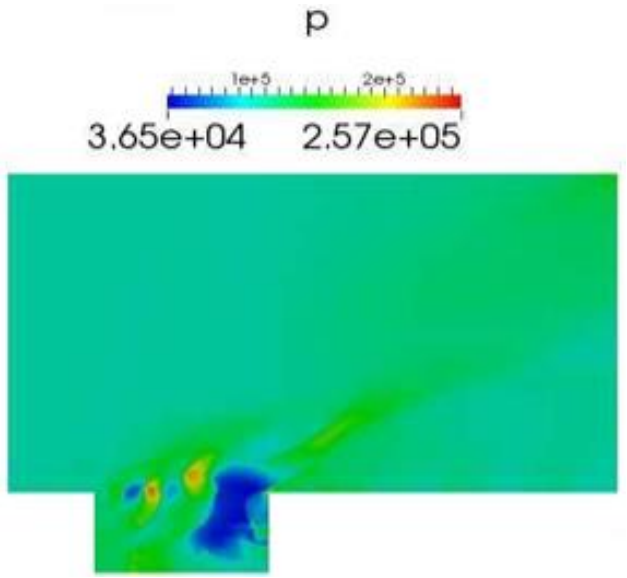

Fig 3. Pressure field at time, t = 0.2 sec

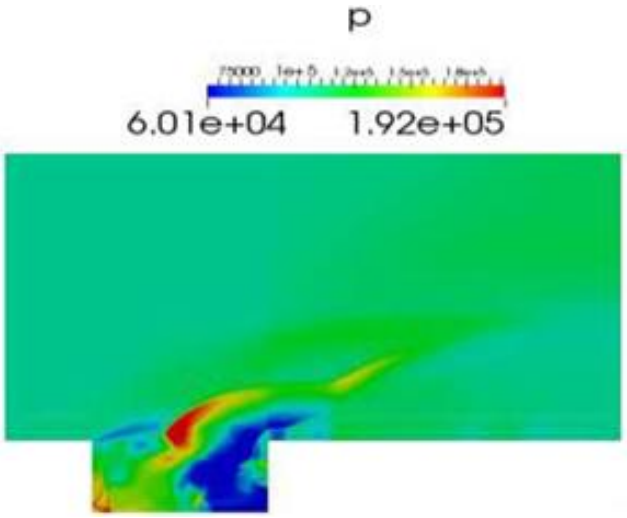

Fig 4. Pressure field at time, t = 0.4 sec

6.2. Comparisons with other numerical and experimental results

6.2.1. Comparison of coefficient of pressure (Cp)

The comparison has been made for the bottom wall of the cavity. The coefficient of pressure at the stated cavity wall is illustrated in figure 5. Moreover, the coefficient of pressure on the said cavity wall is found to be in qualitative agreement with the experimental data and numerical simulation predictions available in literature. The difference in the results from the experimental data of Kaufman et al. is due to the numerical errors introduced during the simulation process. Furthermore, the difference from the Vijaykrishnan investigational work is due to the three-dimensionality effect and also the difference from the Rizzetta investigational work is due to the difference in the Mach number.

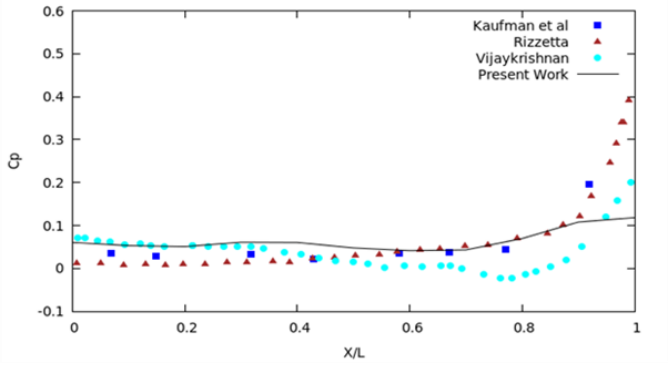

Fig 5. Coefficient of pressure at the centreline of the bottom wall of the cavity

6.2.2. Comparison of overall sound pressure level

The comparison has also been made with the OASPL (Overall Sound Pressure Level) distributions along the bottom wall of the cavity. The OASPL is defined as:

$$OASPL = 10\, log_{10}(\overline{p_d^2}/q^2) \quad (13)$$

Where,

$$\overline{p_d^2} = \frac{1}{t_f - t_i}\int_{t_i}^{t_f}(p-\bar{p})^2\, dt \quad (14)$$

q is the acoustic sound reference level with a value of 2×10^{-5} Pa

$\bar{p}$ is the time-averaged static pressure

t_f and t_i are the initial and final times, respectively

The OASPL distribution is calculated to be approximately 30 dB higher than the experimental data. The OASPL distribution at the stated cavity wall is depicted in figure 6. Nevertheless, the trend is similar to the investigational works done by the other researchers. However, the trend is very similar to the Kaufman et al. and Rizzetta investigational works rather than Vijaykrishnan investigational work. The sound pressure level experienced by the aft wall is nearly 10-15 dB higher than the front wall. The OASPL distribution at the bottom wall is over-predicted (from both Kaufman et al. and Rizzetta investigation results) by nearly 20-40 dB between aft and front walls. However, the over-prediction from Vijaykrishnan investigational work is nearly 40-60 dB between aft and front walls. In addition, from the present investigation, the predicted sound pressure level at the centreline of the bottom wall of the cavity appears to be nearly constant throughout.

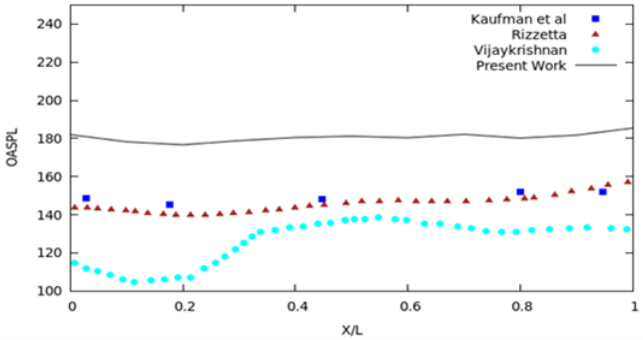

Fig 6. OASPL distribution at the centreline of the bottom wall of the cavity

7. CONCLUSIONS

In the present research work, the numerical simulations have been performed for supersonic flow over a three-dimensional open cavity. The cavity has length-to-depth ratio of 2 and the Mach number of the free-stream is 2.0. The simulations are carried out by using LES based Smagorinsky model for the stated cavity. The numerical simulation results are presented in the form of both cavity flow-field and aeroacoustic analyses. Furthermore, the aeroacoustic analysis is also represented in the form of both coefficient of pressure (Cp) and overall sound pressure level (OASPL). The present numerical simulation predictions are compared with both experimental data and numerical simulation predictions available in the literature. The LES model is able to predict all the main flow features of the cavity. In addition, there is qualitative agreement of the coefficient of pressure with the experimental data and the numerical simulation results reported (in the literature) by the other investigators for supersonic flow over the said cavity. On the other hand, the overall sound pressure level is over-predicted by 30-50 dB. Besides, the feedback loop mechanism of the cavity has also been described. Pretty large pressure fluctuations are witnessed inside the cavity and hence these necessitate to be supressed. However, the attachment of a spoiler in the form of one-fourth of a cylinder at the leading edge of the cavity is also planned for future to alter the flow features inside the cavity which can suppress/reduce both inside pressure oscillations and overall sound pressure level.

REFERENCES

[1] Heller, H. H., Holmes, D. G., & Covert, E. E. (1971). Flow-induced pressure oscillations in shallow cavities. Journal of sound and Vibration, 18(4), 545-553.
[2] Tam, C. K., & Block, P. J. (1978). On the tones and pressure oscillations induced by flow over rectangular cavities. Journal of Fluid Mechanics, 89(02), 373-399.
[3] Kaufman, I. I., Louis, G., Maciulaitis, A., & Clark, R. L. (1983). Mach 0.6 to 3.0 flows over rectangular cavities (No. AFWAL-TR-82-3112). Air force wright aeronautical labs wright-patterson AFB, OH.
[4] Sweby, P. K. (1984). High resolution schemes using flux limiters for hyperbolic conservation laws. SIAM journal on numerical analysis, 21(5), 995-1011.
[5] Rizzetta, D. P. (1988). Numerical simulation of supersonic flow over a three-dimensional cavity. AIAA journal, 26(7), 799-807.
[6] Anderson, J. D., & Wendt, J. F. (1995). Computational fluid dynamics (Vol. 206). New York: McGraw-Hill.
[7] Piomelli, U. (1999). Large-eddy simulation: achievements and challenges. Progress in Aerospace Sciences, 35(4), 335-362.
[8] Hamed, A., Das, K., & Basu, D. (2004). Numerical simulations of fluidic control for transonic cavity flows. AIAA Paper, 429, 2004.
[9] Li, W., Nonomura, T., Oyama, A., & Fujii, K. (2010). LES Study of Feedback-loop Mechanism of Supersonic Open Cavity Flows. AIAA paper, 5112, 2010.
[10] Vijayakrishnan, K. (2014) Unsteady RANS computations of supersonic flow over two dimensional cavity using OpenFOAM-A validation study. AIAA 2014.
[11] Sousa, R. G., et al. (2016). Lid-driven cavity flow of viscoelastic liquids**.** Journal of Non-Newtonian Fluid Mechanics, 234, 129-138, 2016.
[12] Tuerke, F., Pastur, L. R., Sciamarella, D., Lusseyran, F., & Artana, G. (2017). Experimental study of double-cavity flow. Experiments in Fluids, 76, 2017.